Article

Quantitative Profiling of WNT-3A Binding to All Human Frizzled Paralogues in HEK293 Cells by NanoBiT/BRET Assessments

Paweł Kozielewicz,* Rawan Shekhani, Stefanie Moser, Carl-Fredrik Bowin, Janine Wesslowski, Gary Davidson,* and Gunnar Schulte*

Read Online

| ACCESS | | Metrics & More | | Article Recommendations | | Supporting Information |

ABSTRACT: The WNT signaling system governs critical processes during embryonic development and tissue homeostasis, and its dysfunction can lead to cancer. Details concerning selectivity and differences in relative binding affinities of 19 mammalian WNTs to the cysteine-rich domain (CRD) of their receptors—the ten mammalian Frizzleds (FZDs)—remain unclear. Here, we used eGFP-tagged mouse WNT-3A for a systematic analysis of WNT interaction with every human FZD paralogue in HEK293A cells. Employing HiBiT-tagged full-length FZDs, we studied eGFP-WNT-3A binding kinetics, saturation binding, and competition binding with commercially available WNTs in live HEK293A cells using a NanoBiT/BRET-based assay. Further, we generated receptor chimeras to dissect the contribution of the transmembrane core to WNT-CRD binding. Our data pinpoint distinct WNT-FZD selectivity and shed light on the complex WNT-FZD binding mechanism. The methodological development described herein reveals yet unappreciated details of the complexity of WNT signaling and WNT-FZD interactions, providing further details with respect to WNT-FZD selectivity.

KEYWORDS: *WNT, Frizzled, bioluminescence resonance energy transfer (BRET), NanoBiT/BRET, ligand binding, G protein-coupled receptor (GPCR)*
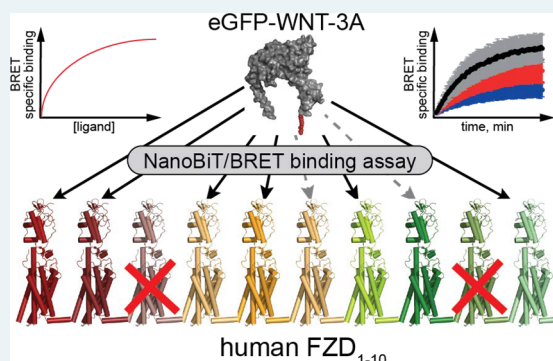
The ten mammalian Frizzleds (FZD_{1-10}) are G protein-coupled receptors (GPCRs) and form—together with Smoothened (SMO)—the class F of GPCRs.[1,2] The 19 different WNT lipoglycoproteins are the main macromolecular ligands of FZDs, interacting with the extracellular cysteine-rich domain (CRD) of the receptor. WNT-FZD signaling orchestrates multiple processes during embryonic development, stem cell regulation, and adult tissue homeostasis.[2] Additionally, aberrant WNT signaling is implicated in tumorigenesis and other pathologies.[3,4] Whereas recent advances have resulted in a better understanding of the underlying mechanisms controlling WNT-induced FZD activation and signal initiation, the relative binding affinities and ligand—receptor selectivity remain largely unknown.[5−13] The quantitative assessment of WNT binding has been limited by the strong lipophilicity of WNTs, which makes their purification challenging and necessitates detergents and serum for solubilization and stabilization of WNTs, respectively.[14,15] Nevertheless, WNT-FZD interactions were studied using biochemical and biophysical assays as well as through the use of *in silico* calculations.[16−22] These studies generally reported WNT-FZD binding affinities in the range of 1−100 nM, which is reasonable when considering the known affinities of proteinaceous ligands to other GPCRs.[23,24] Nevertheless, it remains unclear how these values translate into the

physiological reality, since the local concentration of WNTs at the receptors *in vivo* remains unknown and is likely to be highly context-dependent.[25] Until recently, the assessment of ligand binding was based on WNT binding to the CRD rather than the full-length FZD, or the reported assays were not performed in live cells. However, progress has been made with the use of FRET- and cpGFP-based biosensors to demonstrate WNT-induced FZD conformational dynamics and receptor activation,[7,12,26] where WNT binding to a full-length receptor was reflected by an outward movement of the transmembrane domain TM6. Furthermore, the generation of a functional eGFP-tagged WNT-3A provided for the first time a biologically relevant FZD ligand that could be used as a probe in quantitative binding assays in real-time using living cells.[27,28]

Here, using live cell analysis of transiently transfected HEK293A cells overexpressing HiBiT-tagged FZDs, we provide a comparative assessment of binding affinities of eGFP-WNT-3A to all human FZD paralogues using kinetic
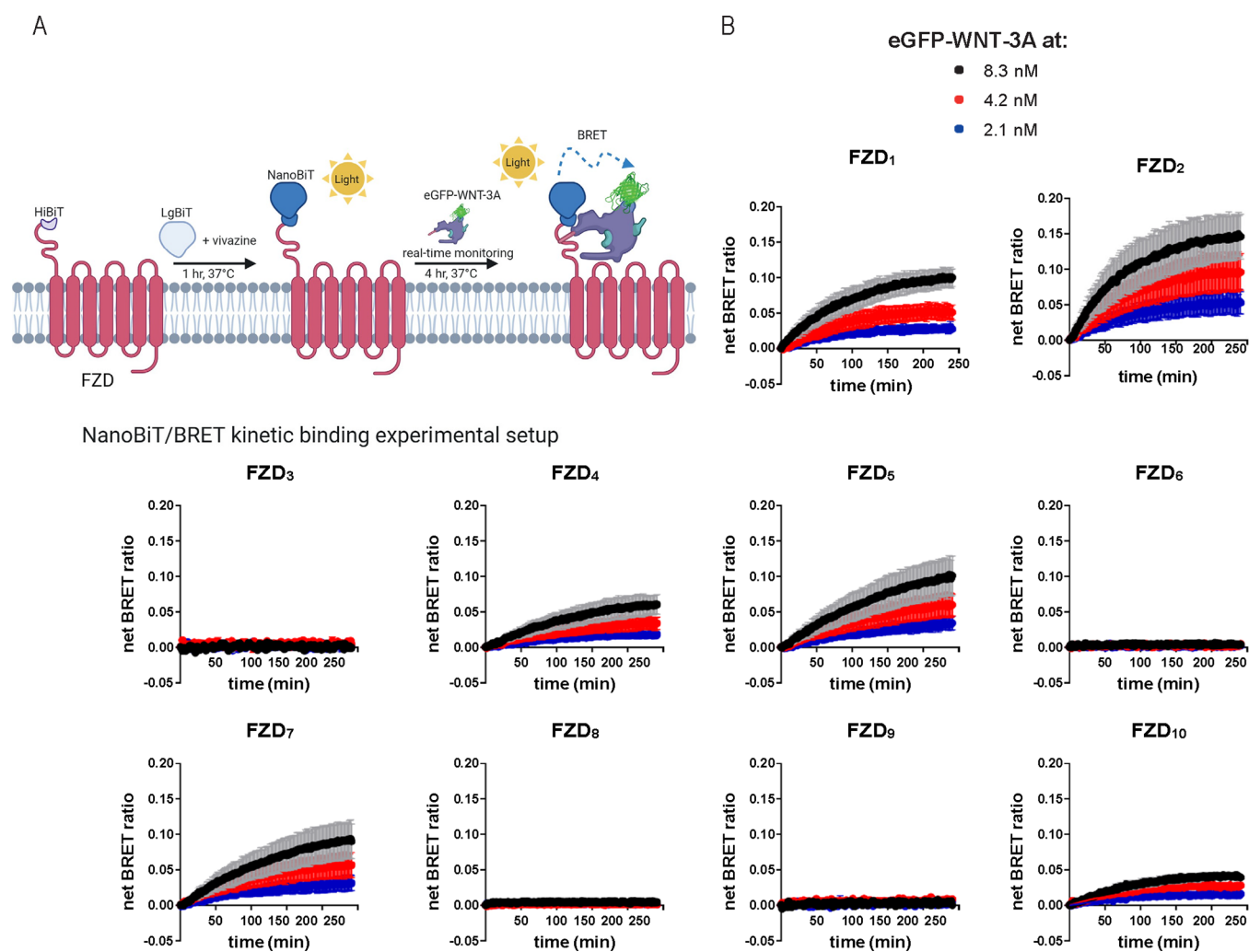
Figure 1. eGFP-WNT-3A binding kinetics. A. The scheme depicts the experimental setup of the NanoBiT/BRET analysis of association kinetics between the HiBiT-tagged FZD and the eGFP-WNT-3A. Created with BioRender.com. B. Association kinetics of the eGFP-WNT-3A to human HiBiT-FZDs were determined by the detection of NanoBiT/BRET in transiently overexpressing living HEK293A cells over time. BRET was sampled once per 90 s for 240 min. Data points are presented as means ± SEM from $n = 3$ individual experiments, fitting a two or more hot ligand concentrations kinetics model. Experiments were performed with eGFP-WNT-3A batch 1.

and saturation binding formats. Furthermore, using a competition binding assay, we have assessed binding affinities of unlabeled, commercially available WNT proteins to FZD_4. Finally, we have also explored the contribution of the FZD transmembrane core for the binding of WNTs to the primary FZD-CRD binding site.[29] Compared with the previously described BRET-based assay for Nluc-FZD_4 and Nluc-FZD_6,[28] we have used a nanoluciferase complementation-based BRET binding approach here, termed NanoBiT/BRET. In this BRET assay format, the fluorescent WNT-3A binds FZDs that are N-terminally tagged with the 11-amino-acid HiBiT peptide. The addition of the complementary LgBiT to the system allows rapid and high-affinity association to the HiBiT peptide, forming a stable NanoBiT moiety with a luciferase activity. This setup allows targeted analysis of cell surface receptors due to the cell impermeability of LgBiT, thereby providing a system with less intracellular background luminescence. This method is a modification of a well-established NanoBRET binding assay to study ligand–receptor association,[30] and has been lately employed to study ligand binding to Class A GPCRs and receptor tyrosine kinases.[31−34] Our results demonstrate that eGFP-WNT-3A interacts with full-length

human FZDs transiently overexpressed in live HEK293A cells in a paralogue selective manner. This concept was expanded to unlabeled WNTs in competition binding experiments suggesting a complex WNT-FZD selectivity profile. The binding data based on full-length FZDs, FZD-CD86, and FZD-FZD chimeras underline the complexity of the WNT-FZD interaction and suggest that the core regions of FZDs may contribute to receptor selectivity.

RESULTS AND DISCUSSION

eGFP-WNT-3A/FZD Binding Kinetics. In order to establish a nanoluciferase complementation-dependent Nano-BiT/BRET binding assay format to study all human FZD paralogues, we generated constructs for all 10 receptors carrying an N-terminal HiBiT tag (Figure S1A,B). Upon transient overexpression in HEK293A cells, all receptor constructs were detected at the cell surface, albeit with varying cell surface expression levels (Figure S1C). Additionally, HiBiT-tagged FZD_1, FZD_2, FZD_4, FZD_5, FZD_7, FZD_8, and FZD_{10} mediated WNT-3A-induced β-catenin-dependent signals as assessed by the TOPFlash reporter assay performed in HEK293T cells devoid of endogenous FZDs (ΔFZD_{1-10}

Table 1. Kinetic and Saturation Binding Parameters of eGFP-WNT-3A Binding to All 10 Human HiBiT-Tagged FZD Paralogues[a]

	FZD$_1$	FZD$_2$	FZD$_3$	FZD$_4$	FZD$_5$	FZD$_6$	FZD$_7$	FZD$_8$	FZD$_9$	FZD$_{10}$
Kinetic binding K_d (nM) ± SEM	29.9 ± 1.5	5.4 ± 0.1	n.d.	9.4 ± 0.5	2.3 ± 0.2	10.2 ± 3.7	2.8 ± 0.2	17.8 ± 4.4	n.d.	4.3 ± 0.3
Saturation binding K_d (nM) ± SEM	36.7 ± 12.7	48.6 ± 8.2	n.d.	17.7 ± 7.2	14.9 ± 7.6	6.5 ± 5.7	24.9 ± 9.9	4.9 ± 3.1	n.d.	21.3 ± 9.0

[a]K_d values are based on data from n = 3–4 individual experiments (shown in Figures 1B and 2B) and shown as a best-fit value ± SEM; n.d. = not determined.
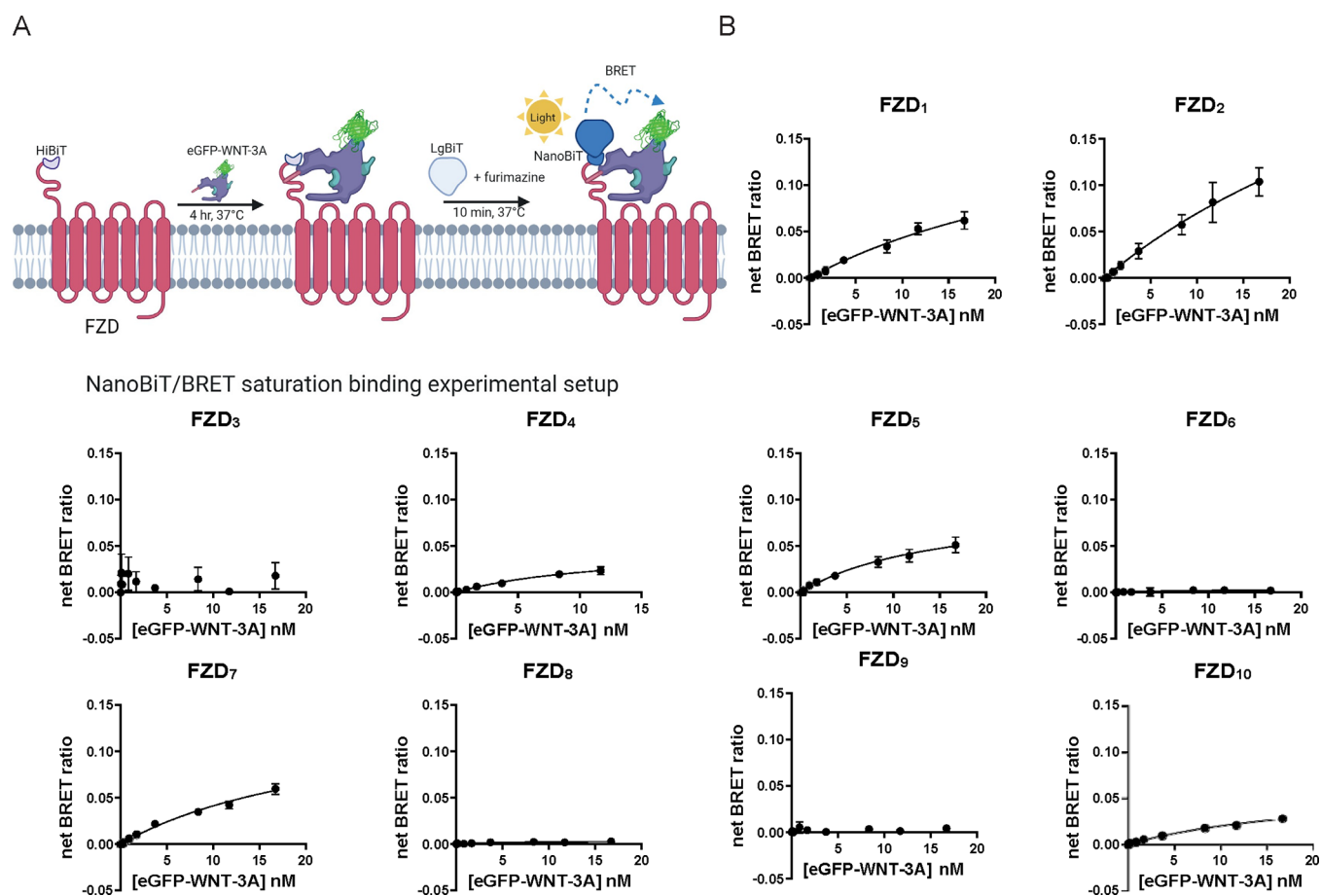

Figure 2. eGFP-WNT-3A saturation binding. A. The scheme depicts the experimental setup of NanoBiT/BRET analysis of equilibrium binding between the HiBiT-tagged FZD and the eGFP-WNT-3A. Created with BioRender.com. B. Saturation binding of the eGFP-WNT-3A to human HiBiT-FZDs was determined by the detection of NanoBiT/BRET in transiently overexpressing living HEK293A cells following 240 min incubation. Data points are presented as means ± SEM from n = 4 individual experiments, fitting a one-site specific model models. Experiments were performed with eGFP-WNT-3A batch 1.

HEK293T cells, Figure S1D[25]). In contrast, FZD$_3$, FZD$_6$, and FZD$_9$ could not transduce WNT-3A-induced activation of this pathway, similar to what has been reported previously, yet with differing results for FZD$_9$.[28,35−38] Having verified the sequence and functionality of the HiBiT-tagged FZD constructs, HEK293A cells transiently overexpressing these FZDs were used in kinetic binding experiments. For these experiments, cells were first incubated with the complementary LgBiT protein and the luciferase substrate vivazine, and after 1 h, eGFP-WNT-3A was added to final concentrations of 2.1, 4.2, or 8.3 nM, and BRET readings were taken over a 4 h period at 37 °C (Figure 1A). The concentrations used for eGFP-WNT-3A were dictated by the maximal concentration that could be obtained for the eGFP-WNT-3A preparations and the assay format. We detected a saturable net BRET ratio indicative of

eGFP-WNT-3A specific binding to HiBiT-tagged FZD$_1$, FZD$_2$, FZD$_4$, FZD$_5$, FZD$_7$, and FZD$_{10}$, with K_d values varying from 2.3 to 29.9 nM (Figure 1B, Table 1). In line with the TOPFlash data, no concentration-dependent increase in receptor−ligand BRET was detected for FZD$_3$ and FZD$_9$. Interestingly, FZD$_8$, which maintained a strong WNT-3A-induced TOPFlash activity, and to a lesser extent FZD$_6$, displayed very low but detectable binding that could be fitted to association curves over time (Figure S2A).

eGFP-WNT-3A/FZD Binding Affinity at Equilibrium. To define saturation binding affinity of eGFP-WNT-3A, we incubated human HiBiT-FZDs with a full concentration range (16.7 pM to 16.7 nM) of eGFP-WNT-3A for 240 min at 37 °C (Figure 2A). The net BRET ratio representing ligand−receptor binding increased in a clear, concentration-dependent manner
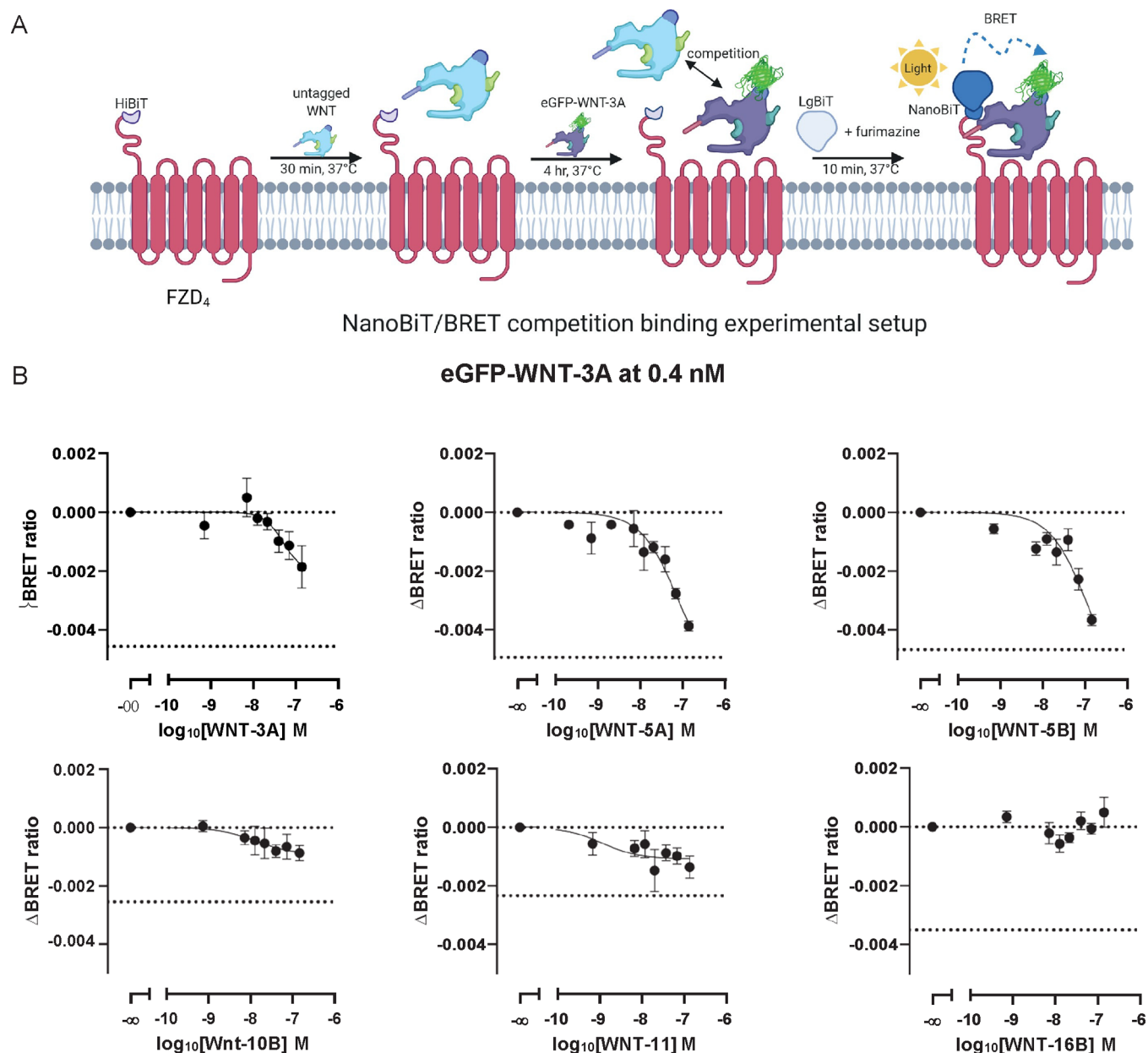
Figure 3. Competition binding between eGFP-WNT-3A and untagged WNTs at FZD_4. A. The scheme depicts the experimental setup of NanoBiT/BRET analysis of competition binding between the eGFP-WNT-3A and commercially available untagged WNT-3A, WNT-5A, WNT-5B, WNT-10B, WNT-11, and WNT-16B. Created with BioRender.com. B. FZD_4 binding of eGFP-WNT-3A at 0.4 nM in the presence of increasing concentrations of the untagged WNTs was determined by the detection of NanoBiT/BRET in transiently overexpressing living HEK293A cells following 240 min incubation. Data points are presented as means ± SEM from $n = 3-6$ individual experiments, fitting a three- or four-parameter model. Upper dashed line indicates the BRET ratio of eGFP-WNT-3A-only treated cells; lower dashed line indicates the BRET ratio of ligand-untreated cells (BRET donor only). Experiments were performed with eGFP-WNT-3A batch 2.

for FZD_1, FZD_2, FZD_4, FZD_5, FZD_7, and FZD_{10}. Unfortunately, using transient overexpression of HiBiT-FZDs in HEK293A cells and the eGFP-WNT-3A with a limited maximal concentration in the conditioned medium, binding curves did not reach maximal asymptotic values but only came to near-saturable levels (Figure 2B). Again, detection of binding of eGFP-Wnt-3A to FZD_6 and FZD_8 was only marginally above background levels, as the net BRET values were low (Figure S2B). Similar to the kinetic binding assays, no quantifiable eGFP-WNT-3A binding was detected for FZD_3 or FZD_9. The affinities of eGFP-WNT-3A/FZD interactions were determined from linear regression curves showing near-

saturable binding,[39] and the K_d values are shown in Table 1. The reported saturation binding affinity values range from 4.9 to 48.6 nM, and they are in good agreement with the K_d values determined with kinetic binding for FZD_1, FZD_4, and FZD_6. The degree of agreement is, however, only fair for FZD_5, FZD_8, and FZD_{10} and relatively poor for FZD_2 and FZD_7. Taken together, these kinetic and saturation binding data are in line with our previous results using fluorescence microscopy analysis, where no eGFP-WNT-3A association could be observed with C-terminally mCherry-tagged FZD_6, and only a very weak association with FZD_8 and FZD_9 (FZD_3 was not used).[28] Although this fluorescence imaging-based method

Table 2. Binding Properties of Various FZD Ligands in Competition with eGFP-WNT-3A Binding (0.4 nM) to HiBiT-FZD$_4$[a]

	WNT-3A	WNT-5A	WNT-5B	WNT-10B	WNT-11	WNT-16B
Competition binding pK_i ± SEM	7.26 ± 0.35	7.08 ± 0.21	6.93 ± 0.25	7.87 ± 0.55	8.90 ± 0.66	n.d.
ΔBRET ± SEM	−0.002 ± 0.001	−0.004 ± 0.0002	−0.004 ± 0.0002	−0.001 ± 0.0003	−0.001 ± 0.0004	n.d.
0.4 nM eGFP- WNT-3A binding displaced (%)	40.8	78.4	78.3	34.5	58.4	n.d.

[a]Data are based on n = 3−6 individual experiments presented in Figure 3B. pK_i values are presented as a best-fit value ± SEM; n.d. = not determined.

could provide an estimate of the relative ability of eGFP-WNT-3A to associate with different FZDs, accurate quantification of the binding affinities was not possible. Also, in that study, ΔFZD$_{1-10}$ HEK293$^{GFP-free}$ cells overexpressing FZD$_8$-mCherry (but not FZD$_6$-mCherry), showed very faint binding of eGFP-WNT-3A, and this is also in agreement with the HiBiT-tagged system used here, which can detect very low level, but specific, binding to FZD$_8$ (Figure S2). This is in agreement with a recent report claiming that ligand−receptor interaction using the HiBiT-tagged system allows detection of very weak interactions.[32] Furthermore, in the case of FZD$_6$, there are differences in reports of its ability to bind or respond to WNT-3A. Biochemical experiments failed to detect any association between WNT-3A and FZD$_6$-CRD-IgG,[16] and no eGFP-WNT-3A/Nluc-FZD$_6$ interaction was detected in our previous NanoBRET study.[28] However, it should be noted that, compared with the HiBiT-tagged systems, binding analyses with Nluc-tagged receptors can display reduced sensitivity for detection of weak interactions, as recently discussed.[32] On the other hand, recombinant human WNT-3A induced a conformational change in FZD$_6$[12] and affected the mobility of the receptor in the cell membrane as assessed by fluorescence recovery after photobleaching assay.[40] Finally, the findings with respect to FZD$_8$ are particularly intriguing, given the existing structural information on the WNT-3A-FZD$_8$ CRD complex.[41] It is currently unclear why such discrepancies exist for these two FZD paralogues.

In order to directly compare NanoBiT/BRET and Nano-BRET binding assay formats, we used Nluc-FZD$_4$ and HiBiT-FZD$_4$ constructs for saturation binding (Figure S3A−C). NanoBiT/BRET experiments were performed in two different experimental paradigms, where LgBiT protein was added either directly after (setup 1, used throughout this study Figure S3B and Figure 2A) or for 10 min before (setup 2, Figure S3C) the 4 h incubation with eGFP-WNT-3A. This allowed us to test for any potential steric hindrance of WNT binding to FZD caused by the presence or complementation of nanoluciferase. In these comparisons, although the differences in K_d values were apparent, they did not reach statistical significance (Nluc-FZD$_4$ K_d (nM) ± SEM = 7.6 ± 3.6; HiBiT-FZD$_4$ setup 1 K_d (nM) ± SEM = 11.9 ± 3.6; HiBiT-FZD$_4$ setup 2 K_d ± SEM (nM) = 20.4 ± 7.6). Furthermore, eGFP-WNT-3A binding to Nluc-FZD$_4$ (Figure S3A) resulted in lower maximal BRET (BRET$_{max}$) compared to either of the two HiBiT-FZD$_4$ binding setups (Figure S3B,C) at similar luminescence levels (Nluc-FZD$_4$ BRET$_{max}$ ± SEM = 0.026 ± 0.006 vs HiBiT-FZD$_4$ setup 1 BRET$_{max}$ ± SEM = 0.049 ± 0.005, P = 0.0484; vs HiBiT-FZD$_4$ setup 2 BRET$_{max}$ ± SEM = 0.049 ± 0.004, P = 0.0349). This suggests that intracellular luminescence originating from receptors that are not accessible for the ligand reduces the assay's dynamic range (see Figure S3D for expression analysis). In support of our choice to change from NanoBRET to the NanoBiT/BRET experimental

setup, a recent study has shown that affinity measurements obtained from NanoBRET binding assays were generally less consistent in comparison with NanoBiT/BRET analyses.[32]

eGFP-WNT-3A Competition Binding with Untagged WNTs at FZD$_4$. With the aim to understand the competitive nature of eGFP-WNT-3A binding to FZD, we combined eGFP-WNT-3A with increasing concentrations of several commercially available and purified untagged WNT proteins: WNT-3A, WNT-5A, WNT-5B, WNT-10B, WNT-11, and WNT-16B. Again, we have used HiBiT-FZD$_4$ as our model receptor. In this assay setup, HEK293A cells transiently overexpressing HiBiT-FZD$_4$ were preincubated with the untagged WNTs for 30 min before addition of eGPF-WNT-3A to a final concentration of 0.4 nM. Cells were then incubated for a further 4 h to allow a competitive equilibrium to be reached before addition of LgBiT and subsequent BRET measurement (Figure 3A). The results of these experiments are shown in Figure 3B and summarized in the Table 2, and show that the untagged WNTs competitively displaced eGFP-WNT-3A from FZD$_4$ with different affinities and capacities. Interestingly, WNT-10B and WNT-11 had the highest affinities, but they showed moderate BRET signal decrease as indicated by remaining residual BRET. Intriguingly, WNT-3A presented higher binding affinity (lower K_d) but caused a lower reduction of BRET than WNT-5A and WNT-5B. WNT-16B did not compete with eGFP-WNT-3A in this FZD$_4$-based assay. These results are in fair agreement with the recently published potencies and efficacies of WNTs in eliciting conformational changes in FZD$_4$-cpGFP biosensor except for WNT-5B.[12] Nevertheless, a similar rank order of affinities was obtained for WNT-3A, WNT-5A, and WNT-5B in binding to the isolated FZD$_4$ CRD.[17] Obviously, the insights into the mechanism of WNT−WNT competition for the primary binding site at FZDs remain obscure. We can only speculate that the process of functional ligand binding is more complex than for small-molecule ligands and other GPCRs. Along these lines, FZD oligomers associate or dissociate upon ligand addition,[42−44] adding to the complexity of ligand binding analysis.[45] Additionally, FZD coreceptors and various regulators could alter WNT interactions with FZD in HEK293 cells.[25]

Binding of eGFP-WNT-3A to FZD Chimeras. WNTs directly engage the CRD through protein−protein and protein−lipid interactions.[41,46] However, it remains unclear whether non-CRD domains of FZDs contribute to WNT-FZD interaction.[20] It has been hypothesized that the CRD simply serves the purpose of binding WNTs in order to bring them in close proximity with the receptor for additional binding/activation mechanisms.[47] Indeed, the long and flexible nature of the linker connecting the CRD of FZDs to TM1 would tend to support such a hypothesis.[48] The role of the FZD transmembrane domains in ligand binding, complex formation, receptor conformational changes, and signal transduction has
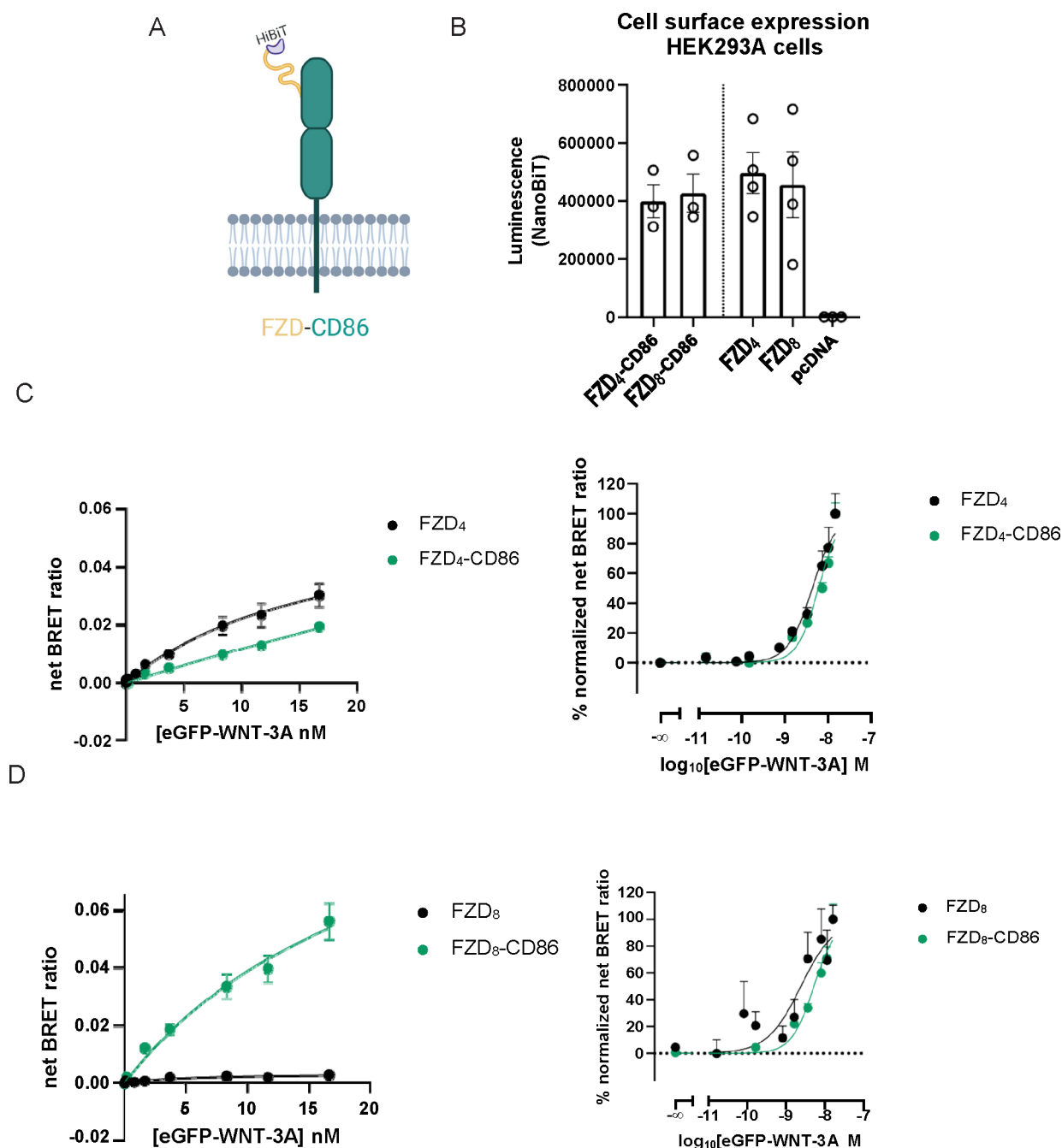
Figure 4. eGFP-WNT-3A binding to FZD-CD86 chimeras. A. The cartoon representations of the FZD-CD86 fusion proteins used in this study. eGFP-WNT-3A binding at equilibrium was assessed as depicted in Figure 2A. Created with BioRender.com. B. Cell surface expression of HiBiT-tagged FZD-CD86 chimeras as measured by NanoBiT luminescence (from the experiments summarized in Figure 2B and parts C−D). Data are presented as means ± SEM from $n = 3-4$ individual experiments. Expression data of FZD_4, FZD_8, and pcDNA are also depicted in SI Figure 1C. C. Saturation binding of eGFP-WNT-3A at FZD_4-CD86 and FZD_4 (data also present in Figure 2B) was determined by the detection of NanoBiT/BRET in transiently overexpressing living HEK293A cells following 240 min incubation. Data points are presented as means ± SEM from $n = 3-4$ individual experiments. eGFP-WNT-3A batch 1 was used in these experiments. D. Saturation binding of eGFP-WNT-3A at FZD_8-CD86 and FZD_8 (data also present in Figure 2B) was determined by the detection of NanoBiT/BRET in transiently overexpressing living HEK293A cells following 240 min incubation. Data points are presented as means ± SEM from $n = 3-4$ individual experiments. eGFP-WNT-3A batch 1 was used in the experiments. Linear scale data are fitted to a one-site specific binding model. Logarithmic-scale data are fitted to a normalized three- or four-parameter model. The right plot in every panel shows data normalized between 0% ($BRET_{min}$) and 100% ($BRET_{max}$) for each studied construct.

been a subject of debate.[5,8,9,49−52] Here, we seek to obtain a more mechanistic insight into the contribution of the transmembrane core to eGFP-WNT-3A binding. To this end, we generated two chimeric proteins fusing the N-terminal domain (NTD; CRD + linker) of one FZD with an unrelated CD86 single transmembrane domain spanning protein (Figure 4A). Specifically, we generated FZD_4-CD86 and FZD_8-CD86 chimeric proteins (Figure S4A). In this manner, we aimed to study the effect of a FZD core on eGFP-WNT-3A binding to the CRD. We validated the chimeras with regard to proper membrane trafficking upon transient overexpression in HEK293A cells and detected no difference in surface

expression levels between FZD-CD86 and wild-type (WT) FZDs (Figure 4B).

In the NanoBiT/BRET binding experiments with the FZD$_4$-CD86 chimera, we could detect a concentration-dependent increase in the BRET signal indicative of eGFP-WNT-3A binding. Interestingly, eGFP-WNT-3A interacted with FZD$_4$-CD86 with a visibly lower affinity (higher K_d) and a visibly lower maximal BRET (at the fixed concentrations used) than for an intact FZD$_4$ protein (FZD$_4$-CD86 $K_d \pm$ SEM (nM) = 141.9 ± 181.5, P = 0.0991; BRET$_{max}$ ± SEM = 0.019 ± 0.001 vs FZD$_4$ BRET$_{max}$ ± SEM = 0.030 ± 0.004, P = 0.0622; Figure 4C). In order to emphasize differences in K_d for the tested receptors, the data were also normalized and are presented in a semilogarithmic presentation in Figure 4C (FZD$_4$-CD86 pK_d ± SEM = 8.19 ± 0.04 vs FZD$_4$ pK_d ± SEM = 8.31 ± 0.05, P = 0.0331). Importantly, differences in BRET$_{max}$ for FZD$_4$-CD86 and FZD$_4$ cannot arise from differences in surface expression levels, as both studied receptors are similarly expressed (P = 0.3324).

Next, we performed a similar analysis for a FZD$_8$-CD86 chimera. eGFP-WNT-3A binding to the chimera FZD$_8$-CD86 compared to FZD$_8$ at similar levels of receptor surface expressions (P = 0.8340; Figure 4B) did not differ in affinity in the analysis of non-normalized data (FZD$_8$-CD86 K_d ± SEM (nM) = 22.9 ± 10.6, P = 0.6668; Figure 4D), but the difference reached statistical significance when comparing the normalized values (P = 0.0390; Figure 4D). Furthermore, the NanoBiT/BRET signal increased significantly when the FZD$_8$ core was replaced by CD86. The NanoBiT/BRET signal (BRET$_{max}$) was in fact comparable to other WNT-3A-binding competent FZDs (FZD$_8$-CD86 BRET$_{max}$ ± SEM = 0.056 ± 0.006 vs FZD$_8$ BRET$_{max}$ ± SEM = 0.003 ± 0.0003, P = 0.0002; Figure 4D and Figure 2). Intriguingly, these findings are the opposite of what we observe for FZD$_4$, where replacing the receptor core with CD86 visibly reduced maximal BRET (Figure 4C). The efficiency of resonance energy transfer depends on both orientation and distance between BRET donor and BRET acceptor.[53] Thus, in the NanoBiT/BRET binding setup, the differences in BRET$_{max}$ can be interpreted as distinct ligand–receptor conformations. This further suggests that the cores of FZD$_4$ and FZD$_8$ can differently contribute to WNT-FZD binding.

In addition to the FZD-CD86 chimeras detailed above, we also generated FZD-FZD chimeras. Specifically, we constructed FZD$_4$-FZD$_6$, FZD$_4$-FZD$_8$, FZD$_5$-FZD$_6$, FZD$_5$-FZD$_7$, and FZD$_6$-FZD$_4$ chimeric proteins (Figure S4B). In this manner, we have used at least one FZD paralogue from every FZD homology cluster. The transmembrane cores of FZD$_6$ and FZD$_8$ were selected to test whether they negatively affect eGFP-WNT-3A binding to the CRD of FZD$_4$ and FZD$_5$. On the other hand, the FZD$_7$ core was chosen to assess if it positively modulates ligand binding to the CRD of FZD$_5$. The rationale for this selection was based on the very weak NanoBiT/BRET signal seen for eGFP-WNT-3A binding to FZD$_6$ and FZD$_8$, and strong NanoBiT/BRET signal of eGFP-WNT-3A/FZD$_7$ association in the two assay paradigms described in this study (Figure 1B and Figure 2B). Additionally, the FZD$_6$ core was replaced with the FZD$_4$ core to assess whether eGFP-WNT-3A binding to FZD$_6$ CRD would increase upon insertion of a core from an eGFP-WNT-3A binding-competent FZD paralogue (Figure 1B and Figure 2B). We validated the chimeras with regard to their proper membrane trafficking upon transient overexpression in

HEK293A cells and detected that the FZD-FZD chimera proteins are relatively poorly expressed on the cell surface compared to WT receptors (Figure S4C). Binding affinities of fluorescent propranolol to HiBiT-tagged β2-adrenergic receptors vary depending on the protein expression levels, with higher expression levels generally resulting in slightly elevated K_d values (lower affinity).[32] Furthermore, binding affinities of DKK1-eGFP proteins to the WNT coreceptor LRP6-mCherry measured by dual-color axial line-scanning FCS (axial lsFCS) were higher for lower, more physiologically relevant receptor expression levels.[54] Our data for transient overexpression of FZD$_4$ in HEK293A cells mostly support these notions, with some exceptions (Figure S4D). Overall, it needs to be emphasized that although the K_d is a thermodynamic parameter that should be constant for various expression levels, differences in the cellular context may lead to different functionalities of overexpressed receptors present on the cell surface. This in turn can affect the comparative analysis and interpretation of real-time ligand binding data.[54] However, provided the availability of cell surface expression data in the experimental paradigm of the NanoBiT/BRET binding assay, we shed light on a potential role of the receptor core for WNT-CRD binding. Focusing on the FZD$_4$ chimeras, eGFP-WNT-3A bound with a significantly higher affinity (lower K_d) to the FZD$_4$-FZD$_6$ and the FZD$_4$-FZD$_8$ chimeras compared to full-length FZD$_4$ (FZD$_4$-FZD$_6$ K_d ± SEM (nM) = 3.5 ± 1.8, P = 0.0255; FZD$_4$-FZD$_8$ K_d ± SEM (nM) = 2.9 ± 1.3, P = 0.0371; Figure S4E). Interestingly, BRET$_{max}$ values were visibly or significantly lower for both weakly expressed FZD$_4$-FZD chimeras than for the intact FZD$_4$ (FZD$_4$-FZD$_6$ BRET$_{max}$ ± SEM = 0.021 ± 0.003, P = 0.0828; FZD$_4$-FZD$_8$ BRET$_{max}$ ± SEM = 0.010 ± 0.001, P = 0.0192).

Additionally, our data showed that in comparison to WT FZD$_5$, eGFP-WNT-3A binding to FZD$_5$-FZD$_6$ occurred with only visibly higher affinity, but this difference did not reach statistical significance (FZD$_5$-FZD$_6$ K_d ± SEM (nM) = 4.4 ± 1.5, P = 0.0638; Figure S4F). Next, the affinity of eGFP-WNT-3A binding to FZD$_5$-FZD$_7$ was also not significantly different compared with WT FZD$_5$ (FZD$_5$-FZD$_7$ K_d ± SEM (nM) = 5.0 ± 2.4, P = 0.2622; Figure S4F). Moreover, the differences in BRET$_{max}$ did not reach statistical significance (FZD$_5$-FZD$_6$ BRET$_{max}$ ± SEM = 0.080 ± 0.014, P = 0.1715; FZD$_5$-FZD$_7$ BRET$_{max}$ ± SEM = 0.098 ± 0.026, P = 0.2046; FZD$_5$ BRET$_{max}$ ± SEM = 0.051 ± 0.009).

In addition, our data indicated that eGFP-WNT-3A bound to FZD$_6$-FZD$_4$ with the same affinity (FZD$_6$-FZD$_4$ K_d ± SEM (nM) = 5.8 ± 3.4, P = 0.9695; Figure S4G) as to FZD$_6$ but with a significant, over 10-fold increase in the maximal BRET signal (FZD$_6$-FZD$_4$ BRET$_{max}$ ± SEM = 0.030 ± 0.006 vs FZD$_6$ BRET$_{max}$ ± SEM = 0.002 ± 0.001, P = 0.056) arguing that the FZD$_6$CRD can efficiently bind eGFP-WNT-3A in the context of a different receptor core. As mentioned before, it needs to be emphasized that receptor expression levels can affect ligand–receptor interaction. Along these lines, in classical BRET titration experiments, increasing BRET donor amounts (by increasing plasmid DNA amounts) with constant BRET acceptor levels (unchanged plasmid DNA amounts) leads to a decrease in BRET$_{max}$ signal for specific donor–acceptor interactions.[55] In contrast, no such relationship was found in our FZD-CD86 and FZD-FZD NanoBiT/BRET binding experiments, further supporting the notion that the FZD core has a differential role in WNT binding depending on the FZD paralogue.

Here, we have used the NanoBiT/BRET system to analyze the contribution of the FZD seven-transmembrane-spanning core to eGFP-WNT-3A binding to the CRD. We show that swapping the receptor core can have a substantial effect on the affinity or maximal BRET of eGFP-WNT-3A binding in the NanoBiT/BRET read-out. Our data, particularly from the FZD-CD86 experiments, argue that the seven-transmembrane-spanning core contributes to ligand binding for the tested FZDs, even though the details on the molecular level remain obscure.

This study adds substantial methodological advance to the pharmacological toolbox suitable for the study of the class F GPCRs and their coreceptors.[28,54,56] We have demonstrated the vast potential of employing fluorescent WNTs and the NanoBiT/BRET binding technique for the pharmacological quantification of WNT-FZD interactions in live HEK293A cells despite the limitations that come with the low concentration of the tracer WNT in the conditioned medium preparation. The broader analysis of the selectivity of ligand–receptor interactions, WNT binding in the presence or absence of either FZD coreceptors, FZD-binding intracellular transducer proteins and at different FZD expression levels, can now be further investigated to understand the pluridimensionality of WNT-FZD system in a more physiologically relevant cell system.

■ EXPERIMENTAL SECTION

Cell Culture and Ligands. HEK293A cells (ATCC), HEK293F (Thermo Fisher Scientific, Waltham, MA, USA), HEK293T (DSMZ ACC-635), and ΔFZD_{1-10} HEK293T cells[25] were cultured in DMEM supplemented with 10% FBS, 1% penicillin/streptomycin, and 1% L-glutamine (all from Thermo Fisher Scientific, Waltham, MA, USA) in a humidified CO_2 incubator at 37 °C. All cell culture plastics were from Sarstedt (Nümbrecht, Germany), unless otherwise specified. The absence of mycoplasma contamination was routinely confirmed by PCR using 5′-GGCGAATGGGTGAGTAACA-CG-3′ and 5′-CGGATAACGCTTGCGACTATG-3′ primers detecting 16 S rRNA of mycoplasma in the media after 2−3 days of cell exposure. Untagged human WNT-3A, human/mouse WNT-5A, human WNT-5B, human WNT-10B, human WNT-11, and human WNT-16B were all from RnD Systems/Biotechne (#5036-WN, #645-WN, #7347-WN, #7196-WN, #6179-WN, and #7790-WN, Minneapolis, MI, USA). WNTs were dissolved at 100 μg/mL in filter-sterilized 0.1% BSA/PBS and stored at 4 °C. Molecular weights of the WNTs were as per supplier's datasheets. Porcupine inhibitor C59 was from Abcam (#ab142216, Cambridge, UK).[57] C59 was dissolved in DMSO at 5 mM and stored at −20 °C. The serial dilutions of WNTs were prepared in the protein-low binding tubes (Eppendorf, Hamburg, Germany).

Preparation of eGFP-WNT-3A CM. HEK293F suspension cells growing in serum-free Expi293 expression medium (60 mL, 2.5×10^6 cells/mL) were cotransfected with 10 μg of either *pCS2+-WNT-3A* or *pCS2+-eGFP-WNT- 3A* together with 50 μg of *pCMV-His-Afamin* plasmid using ScreenFect UP-293 (ScreenFect GmbH, Eggenstein-Leopoldshafen, Germany) according to the manufacturer's instructions. The corresponding control CM was generated from cells transfected with *pCS2+* plasmid.

Cells were first cleared from the HEK293F CM by centrifugation at 260 *g* (1200 rpm) for 10 min and then at 2800 *g* (4000 rpm) for 30 min to remove any remaining

cellular debris and insoluble material. This "raw" CM then was concentrated 5-fold using Vivaspin turbo 15 centrifugal concentrators (30,000-molecular-weight-cutoff, Satorius AG, Göttingen, Germany) and exchanged to the desired cell culture medium using Sephadex G-25 PD10 desalting columns (GE Healthcare Bio-Science, Freiburg, Germany). The final concentration and integrity of eGFP-WNT-3A in the CM samples were determined using ELISA (GFP ELISA kit, #ab171581, Abcam) and SDS-PAGE/Western Blot analysis, respectively. Two eGFP-WNT-3A batches (eGFP-WNT-3A batch 1 final concentration: 16.7 nM; eGFP-WNT-3A batch 2 final concentration: 16.2 nM) were used in this study. Current WNT purification methods allow only limited WNT concentration to be obtained from CM.[58] For validation of the eGFP-WNT-3A batches, please see Figure S5.

Plasmids. Generation of $HiBiT-FZD_4$, $HiBiT-FZD_6$, and $Nluc-FZD_4$ has been described previously.[28] Gibson cloning was used to generate other HiBiT-tagged receptor constructs using HiBiT-tagged backbone from $HiBiT-FZD_4$ containing a $5-HT_{3A}$ signal sequence. To generate chimeras, the N-terminal domains (NTD; CRD with a linker region) and the transmembrane cores were defined according to Frizzled structures predicted on GPCRdb (http://www.gpcrdb.org), and the constructs were generated with Gibson cloning. Nluc-CD86 used to generate FZD-CD86 chimeras was from Martin J. Lohse (Max-Delbrueck Center for Molecular Medicine, Berlin, Germany). Frizzled and CD86 signal peptides were defined with SignalP-5.0 Server (http://www.cbs.dtu.dk/services/SignalP/). The constructs were validated by sequencing (Eurofins GATC, Konstanz, Germany). The details of the constructs used in this study are presented in Figure S1A,B and Figure S4A.

NanoBiT/BRET Binding. HEK293A cells were transiently transfected in suspension using Lipofectamine 2000 (Thermo Fisher Scientific, Waltham, MA, USA). A total of 4×10^5 cells were transfected in 1 mL with 1000 ng of HiBiT-tagged FZDs or 10 ng of $Nluc-FZD_4$ plasmid DNA. The cells (50 μL) were seeded onto a poly(D-lysine)-coated black 96-well cell culture plate with a solid flat bottom (Greiner BioOne). Next, 50 μL of complete DMEM medium was added to each well. Forty-eight hours post-transfection, the cells were washed once with 200 μL of Hanks' balanced salt solution (HBSS; HyClone). In the kinetic binding experiments, the cells were preincubated with 50 μL of a mix of Nluc substrate vivazine (1:50 dilution; #N2581, Promega, Fitchburg, WI, USA) and LgBiT (1:100 dilution; #N2421, Promega, Fitchburg, WI, USA) in a complete, nonphenol red DMEM (HyClone) supplemented with 10 mm HEPES for 1 h at 37 °C without CO_2. Subsequently, 50 μL of eGFP-WNT-3A conditioned medium or control medium supplemented with 5% FBS and 10 mm HEPES was added, and the BRET signal was measured every 90 s for 240 min at 37 °C (161 measurements, no CO_2). In the saturation-binding experiments, the cells were incubated with different concentrations of eGFP-WNT-3A conditioned medium (90 μL) supplemented with 5% FBS and 10 mm HEPES for 240 min at 37 °C with no CO_2. In the competition binding experiments, the cells were preincubated for 30 min at 37 °C with 80 μL of unlabeled WNT proteins at 37 °C with no CO_2. Subsequently, 10 μL of eGFP-WNT-3A at a concentration of 3.6 nM (final concentration of 0.4 nM) were added, and the cells were incubated for further 240 min at 37 °C with no CO_2. Next, for saturation and competition binding experiments, 10 μL of a mix of furimazine (1:10 dilution;

#N2421, Promega, Fitchburg, WI, USA) and LgBiT (1:20 dilution; #N2421, Promega, Fitchburg, WI, USA) was added. For saturation binding experiments with Nluc-FZD$_4$ furimazine was used at 1:1000 final dilution (#N1572, Promega, Fitchburg, WI, USA) and no LgBiT was added. The cells were incubated for another 10 min at 37 °C with no CO_2 before the BRET measurements. The BRET ratio was determined as the ratio of light emitted by eGFP (energy acceptor) and light emitted by HiBiT-FZD$_{1-10}$ or Nluc-FZD$_4$ (energy donors). The net BRET ratio was calculated as the difference in BRET ratio between cells treated with eGFP-WNT-3A, and cells treated with vehicle. ΔBRET ratio in the competition binding experiment was calculated as the difference in BRET ratio of cells treated with vehicle (eGFP-WNT-3A only wells, no ΔBRET) and cells treated with WNTs. The BRET acceptor (bandpass filter, 535−30 nm) and BRET donor (bandpass filter, 475−30 nm) emission signals were measured using a CLARIOstar microplate reader (BMG, Ortenberg, Germany). Cell surface expression of HiBiT-tagged FZDs and total expression of Nluc-FZD$_4$ was assessed by measuring luminescence of vehicle-treated wells (no BRET acceptor) in the NanoBiT/BRET or NanoBRET binding assays, respectively. eGFP fluorescence was measured prior to reading BRET (excitation, 470−15 nm; emission, 515−20 nm).

TOPFlash Reporter Gene Assay. ΔFZD$_{1-10}$ HEK 293T cells were transfected in suspension (4 × 10^5 cells were transfected in 1 mL) with 700 ng of HiBiT-tagged receptor, 250 ng M50 Super 8× TOPFlash (#12456; Addgene, Watertown, MA, USA), and 50 ng pRL-TK Luc (#E2241, Promega, Fitchurg, WI, USA) and seeded (50 μL) onto a poly(D-lysine)-coated white 96-well cell culture plate with a solid flat bottom (Greiner BioOne). Next, 50 μL of complete DMEM medium was added to each well. Twenty-four hours after transfection, the medium was changed to starvation medium (DMEM without FBS) containing either 8.0 nM (300 ng/mL) WNT-3A or vehicle, and 10 nM C59. Twenty-four hours after stimulation, cells were lysed gently shaking with 20 μL 1× Passive Lysis Buffer (#E1910; Promega, Fitchurg, WI, USA) for 15 min. Subsequently, 20 μL of LAR II (Promega, E1910) was added to all wells after which luminescence (580−80 nm) was read, and then 20 μL of Stop & Glo (Promega, E1910) was added to all wells after which luminescence (480−80 nm) was read again with a CLARIOstar microplate reader (BMG, Ortenberg, Germany).

Data Analysis and Statistics. All data were analyzed in GraphPad Prism 8 (San Diego, CA, USA) using built-in equations. All data presented in this study come from n individual experiments (at least three biological replicates) with each individual experiment performed typically in duplicates (technical replicates) for each tested concentration/condition. Data points on the binding curves represent mean ± SEM. Saturation binding curves were fit using one-site-specific or total and nonspecific saturation nonlinear regression models (linear scale for eGFP-WNT-3A concentrations) or normalized three-parameter or normalized four-parameter nonlinear regression models (logarithmic scale for eGFP-WNT-3A concentrations with normalized net BRET ratio). The fitting models were selected based on an extra-sum-of-squares F-test ($P < 0.05$). Kinetic binding data were analyzed using the association model with two or more hot ligand concentrations. Binding affinity values (K_d) are presented as a best-fit K_d with SEM. K_d values were compared using an extra-sum-of-squares F-test ($P < 0.05$). Competition

binding curves were analyzed using a three- or four-parameter nonlinear regression model to obtain equilibrium dissociation constant values pK_i with SEM of unlabeled ligands as per the Cheng−Prusoff equation.[59] Minimal BRET (BRET$_{min}$) and maximal BRET (BRET$_{max}$) were defined as the lowest and highest measured net BRET ratios, respectively. BRET$_{max}$ values were compared using unpaired t-test. TOPFlash and cell surface expression data are presented as mean ± SEM. TOPFlash and cell surface expression data were analyzed for differences with Brown−Forsythe and Welch one-way analysis of variance (ANOVA); ** $P \leq 0.01$, * $P \leq 0.05$.

■ ASSOCIATED CONTENT

ⓈI Supporting Information
The Supporting Information is available free of charge at https://pubs.acs.org/doi/10.1021/acsptsci.1c00084.

> Detailed plasmid information, cell surface expression data, TOPFlash data, NanoBRET vs NanoBiT/BRET binding comparison data, detailed information about FZD-CD86 and FZD-FZD chimeras, eGFP-WNT-3A binding to FZD-FZD chimeras and eGFP-WNT-3A validation PDF)

■ AUTHOR INFORMATION

Corresponding Authors
  Paweł Kozielewicz − *Section of Receptor Biology & Signaling, Dept. Physiology & Pharmacology, Karolinska Institutet, S-17165 Stockholm, Sweden;* ⊙ orcid.org/0000-0003-1414-3566; Email: pawel.kozielewicz@ki.se
  Gary Davidson − *Institute of Biological and Chemical Systems-Functional Molecular Systems (IBCS-FMS), Karlsruhe Institute of Technology (KIT), 76131 Karlsruhe, Germany;* ⊙ orcid.org/0000-0002-2264-5518; Email: gary.davidson@kit.edu
  Gunnar Schulte − *Section of Receptor Biology & Signaling, Dept. Physiology & Pharmacology, Karolinska Institutet, S-17165 Stockholm, Sweden;* ⊙ orcid.org/0000-0002-2700-7013; Email: gunnar.schulte@ki.se

Authors
  Rawan Shekhani − *Section of Receptor Biology & Signaling, Dept. Physiology & Pharmacology, Karolinska Institutet, S-17165 Stockholm, Sweden;* ⊙ orcid.org/0000-0002-4632-2131
  Stefanie Moser − *Institute of Biological and Chemical Systems-Functional Molecular Systems (IBCS-FMS), Karlsruhe Institute of Technology (KIT), 76131 Karlsruhe, Germany;* ⊙ orcid.org/0000-0003-4087-0206
  Carl-Fredrik Bowin − *Section of Receptor Biology & Signaling, Dept. Physiology & Pharmacology, Karolinska Institutet, S-17165 Stockholm, Sweden;* ⊙ orcid.org/0000-0001-9090-9493
  Janine Wesslowski − *Institute of Biological and Chemical Systems-Functional Molecular Systems (IBCS-FMS), Karlsruhe Institute of Technology (KIT), 76131 Karlsruhe, Germany;* ⊙ orcid.org/0000-0003-3674-1372

Complete contact information is available at:
https://pubs.acs.org/10.1021/acsptsci.1c00084

Author Contributions

P.K. and G.S. and G.D. conceived the study, and P.K. and G.S. designed the study. S.M. and J.W. generated and validated the

■ ABBREVIATIONS

CM, conditioned medium; CRD, cysteine-rich domain; eGFP, enhanced green fluorescent protein; FRET, Förster resonance energy transfer; FZD, Frizzled; GPCR, G protein-coupled receptor; HBSS, Hank's balanced salt solution; NanoBiT/BRET, nanoluciferase binary technology/bioluminescence resonance energy transfer; Nluc, nanoluciferase; NTD, N-terminal domain; TCF/LEF, T-cell factor/lymphoid enhancer-binding factor; WNT, WNT/Int-1 family of proteins; WT, wild-type

■ REFERENCES

(1) Foord, S. M., Bonner, T. I., Neubig, R. R., Rosser, E. M., Pin, J. P., Davenport, A. P., Spedding, M., and Harmar, A. J. (2005) International Union of Pharmacology. XLVI. G protein-coupled receptor list. *Pharmacol. Rev.* 57, 279−288.

(2) Schulte, G. (2010) International Union of Basic and Clinical Pharmacology. LXXX. The class Frizzled receptors. *Pharmacol. Rev.* 62, 632−667.

(3) Jung, Y. S., and Park, J. I. (2020) Wnt signaling in cancer: therapeutic targeting of Wnt signaling beyond beta-catenin and the destruction complex. *Exp. Mol. Med.* 52, 183−191.

(4) Burgy, O., and Konigshoff, M. (2018) The WNT signaling pathways in wound healing and fibrosis. *Matrix Biol.* 68−69, 67−80.

(5) Schulte, G., and Kozielewicz, P. (2020) Structural insight into Class F receptors - What have we learnt regarding agonist-induced activation? *Basic Clin. Pharmacol. Toxicol.* 126, 17.

(6) Schulte, G., and Wright, S. C. (2018) Frizzleds as GPCRs - More Conventional Than We Thought! *Trends Pharmacol. Sci.* 39, 828−842.

(7) Kozielewicz, P., Turku, A., Bowin, C. F., Petersen, J., Valnohova, J., Canizal, M. C. A., Ono, Y., Inoue, A., Hoffmann, C., and Schulte, G. (2020) Structural insight into small molecule action on Frizzleds. *Nat. Commun.* 11, 414.

(8) Wright, S. C., Kozielewicz, P., Kowalski-Jahn, M., Petersen, J., Bowin, C. F., Slodkowicz, G., Marti-Solano, M., Rodriguez, D., Hot, B., Okashah, N., et al. (2019) A conserved molecular switch in Class F receptors regulates receptor activation and pathway selection. *Nat. Commun.* 10, 667.

(9) Tsutsumi, N., Mukherjee, S., Waghray, D., Janda, C. Y., Jude, K. M., Miao, Y., Burg, J. S., Aduri, N. G., Kossiakoff, A. A., Gati, C., et al. (2020) Structure of human Frizzled5 by fiducial-assisted cryo- EM supports a heterodimeric mechanism of canonical Wnt signaling. *eLife* 9, 9.

(10) Nygaard, R., Yu, J., Kim, J., Ross, D. R., Parisi, G., Clarke, O. B., Virshup, D. M., and Mancia, F. (2021) Structural Basis of WLS/Evi-Mediated Wnt Transport and Secretion. *Cell* 184, 194−206.

(11) Bowin, C. F., Inoue, A., and Schulte, G. (2019) WNT-3A-induced beta-catenin signaling does not require signaling through heterotrimeric G proteins. *J. Biol. Chem.* 294, 11677−11684.

(12) Schihada, H., Kowalski-Jahn, M., Turku, A., and Schulte, G. (2021) Deconvolution of WNT-induced Frizzled conformational dynamics with fluorescent biosensors. *Biosens. Bioelectron.* 177, 112948.

(13) Ma, W., Chen, M., Kang, H., Steinhart, Z., Angers, S., He, X., and Kirschner, M. W. (2020) Single-molecule dynamics of Dish-evelled at the plasma membrane and Wnt pathway activation. *Proc. Natl. Acad. Sci. U. S. A.* 117, 16690−16701.

(14) Tuysuz, N., van Bloois, L., van den Brink, S., Begthel, H., Verstegen, M. M., Cruz, L. J., Hui, L., van der Laan, L. J., de Jonge, J., Vries, R., et al. (2017) Lipid-mediated Wnt protein stabilization enables serum-free culture of human organ stem cells. *Nat. Commun.* 8, 14578.

(15) Mihara, E., Hirai, H., Yamamoto, H., Tamura-Kawakami, K., Matano, M., Kikuchi, A., Sato, T., and Takagi, J. (2016) Active and water-soluble form of lipidated Wnt protein is maintained by a serum glycoprotein afamin/alpha-albumin. *eLife* 5, 5.

(16) Sato, A., Yamamoto, H., Sakane, H., Koyama, H., and Kikuchi, A. (2010) Wnt5a regulates distinct signalling pathways by binding to Frizzled2. *EMBO J.* 29, 41−54.

(17) Dijksterhuis, J. P., Baljinnyam, B., Stanger, K., Sercan, H. O., Ji, Y., Andres, O., Rubin, J. S., Hannoush, R. N., and Schulte, G. (2015) Systematic mapping of WNT-FZD protein interactions reveals functional selectivity by distinct WNT-FZD pairs. *J. Biol. Chem.* 290, 6789−6798.

(18) Wu, C. H., and Nusse, R. (2002) Ligand receptor interactions in the Wnt signaling pathway in Drosophila. *J. Biol. Chem.* 277, 41762−41769.

(19) Agostino, M., Pohl, S. O., and Dharmarajan, A. (2017) Structure-based prediction of Wnt binding affinities for Frizzled-type cysteine-rich domains. *J. Biol. Chem.* 292, 11218−11229.

(20) Hsieh, J. C., Rattner, A., Smallwood, P. M., and Nathans, J. (1999) Biochemical characterization of Wnt- Frizzled interactions using a soluble, biologically active vertebrate Wnt protein. *Proc. Natl. Acad. Sci. U. S. A.* 96, 3546−3551.

(21) Swain, R. K., Katoh, M., Medina, A., and Steinbeisser, H. (2005) Xenopus frizzled-4S, a splicing variant of Xfz4 is a context-dependent activator and inhibitor of Wnt/beta-catenin signaling. *Cell Commun. Signaling* 3, 12.

(22) Agostino, M., and Pohl, S. O. (2019) Wnt Binding Affinity Prediction for Putative Frizzled-Type Cysteine-Rich Domains. *Int. J. Mol. Sci.* 20, 4168.

(23) Davenport, A. P., Scully, C. C. G., de Graaf, C., Brown, A. J. H., and Maguire, J. J. (2020) Advances in therapeutic peptides targeting G protein-coupled receptors. *Nat. Rev. Drug Discovery* 19, 389−413.

(24) Kaiser, A., and Coin, I. (2020) Capturing Peptide-GPCR Interactions and Their Dynamics. *Molecules* 25, 4724.

(25) Eubelen, M., Bostaille, N., Cabochette, P., Gauquier, A., Tebabi, P., Dumitru, A. C., Koehler, M., Gut, P., Alsteens, D., Stainier, D. Y. R., et al. (2018) A molecular mechanism for Wnt ligand-specific signaling. *Science* 361, eaat1178.

(26) Wright, S. C., Canizal, M. C. A., Benkel, T., Simon, K., Le Gouill, C., Matricon, P., Namkung, Y., Lukasheva, V., Konig, G. M.,

Laporte, S. A., et al. (2018) FZD$_5$ is a Galphaq-coupled receptor that exhibits the functional hallmarks of prototypical GPCRs. *Sci. Signaling* 11, eaar5536.

(27) Takada, R., Mii, Y., Krayukhina, E., Maruyama, Y., Mio, K., Sasaki, Y., Shinkawa, T., Pack, C. G., Sako, Y., Sato, C., et al. (2018) Assembly of protein complexes restricts diffusion of Wnt3a proteins. *Commun. Biol.* 1, 165.

(28) Wesslowski, J., Kozielewicz, P., Wang, X., Cui, H., Schihada, H., Kranz, D., Karuna, M. P., Levin, P., Gross, J. C., Boutros, M., et al. (2020) eGFP-tagged Wnt-3a enables functional analysis of Wnt trafficking and signaling and kinetic assessment of Wnt binding to full-length Frizzled. *J. Biol. Chem.* 295, 8759−8774.

(29) Bazan, J. F., Janda, C. Y., and Garcia, K. C. (2012) Structural architecture and functional evolution of Wnts. *Dev. Cell* 23, 227−232.

(30) Stoddart, L. A., Johnstone, E. K., Wheal, A. J., Goulding, J., Robers, M. B., Machleidt, T., Wood, K. V., Hill, S. J., and Pfleger, K. D. (2015) Application of BRET to monitor ligand binding to GPCRs. *Nat. Methods* 12, 661−663.

(31) Soave, M., Heukers, R., Kellam, B., Woolard, J., Smit, M. J., Briddon, S. J., and Hill, S. J. (2020) Monitoring Allosteric Interactions with CXCR4 Using NanoBiT Conjugated Nanobodies. *Cell Chem. Biol.* 27, 1250−1261.

(32) Boursier, M. E., Levin, S., Zimmerman, K., Machleidt, T., Hurst, R., Butler, B. L., Eggers, C. T., Kirkland, T. A., Wood, K. V., and Friedman Ohana, R. (2020) The luminescent HiBiT peptide enables selective quantitation of G protein-coupled receptor ligand engagement and internalization in living cells. *J. Biol. Chem.* 295, 5124−5135.

(33) Soave, M., Kellam, B., Woolard, J., Briddon, S. J., and Hill, S. J. (2020) NanoBiT Complementation to Monitor Agonist-Induced Adenosine A1 Receptor Internalization. *SLAS Discov* 25, 186−194.

(34) Peach, C. J., Kilpatrick, L. E., Woolard, J., and Hill, S. J. (2021) Use of NanoBiT and NanoBRET to monitor fluorescent VEGF-A binding kinetics to VEGFR2/NRP1 heteromeric complexes in living cells. *Br. J. Pharmacol.*, 1 DOI: 10.1111/bph.15426.

(35) Ring, L., Neth, P., Weber, C., Steffens, S., and Faussner, A. (2014) beta-Catenin-dependent pathway activation by both promiscuous "canonical" WNT3a-, and specific "noncanonical" WNT4- and WNT5a-FZD receptor combinations with strong differences in LRP5 and LRP6 dependency. *Cell. Signalling* 26, 260−267.

(36) Yu, H., Ye, X., Guo, N., and Nathans, J. (2012) Frizzled 2 and frizzled 7 function redundantly in convergent extension and closure of the ventricular septum and palate: evidence for a network of interacting genes. *Development* 139, 4383−4394.

(37) Voloshanenko, O., Gmach, P., Winter, J., Kranz, D., and Boutros, M. (2017) Mapping of Wnt-Frizzled interactions by multiplex CRISPR targeting of receptor gene families. *FASEB J.* 31, 4832−4844.

(38) Karasawa, T., Yokokura, H., Kitajewski, J., and Lombroso, P. J. (2002) Frizzled-9 is activated by Wnt-2 and functions in Wnt/beta-catenin signaling. *J. Biol. Chem.* 277, 37479−37486.

(39) Kenakin, T. *A Pharmacology Primer - Techniques for More Effective and Strategic Drug Discovery*, 5th ed., Fedor, J., Ed.; Academic Press, 2018; pp 85.

(40) Kilander, M. B., Dahlstrom, J., and Schulte, G. (2014) Assessment of Frizzled 6 membrane mobility by FRAP supports G protein coupling and reveals WNT-Frizzled selectivity. *Cell. Signalling* 26, 1943−1949.

(41) Hirai, H., Matoba, K., Mihara, E., Arimori, T., and Takagi, J. (2019) Crystal structure of a mammalian Wnt-frizzled complex. *Nat. Struct. Mol. Biol.* 26, 372−379.

(42) Petersen, J., Wright, S. C., Rodriguez, D., Matricon, P., Lahav, N., Vromen, A., Friedler, A., Stromqvist, J., Wennmalm, S., Carlsson, J., et al. (2017) Agonist-induced dimer dissociation as a macromolecular step in G protein-coupled receptor signaling. *Nat. Commun.* 8, 226.

(43) DeBruine, Z. J., Ke, J., Harikumar, K. G., Gu, X., Borowsky, P., Williams, B. O., Xu, W., Miller, L. J., Xu, H. E., and Melcher, K. (2017) Wnt5a promotes Frizzled-4 signalosome assembly by stabilizing cysteine-rich domain dimerization. *Genes Dev.* 31, 916−926.

(44) Bang, I., Kim, H. R., Beaven, A. H., Kim, J., Ko, S. B., Lee, G. R., Lee, H., Im, W., Seok, C., Chung, K. Y., et al. (2018) Biophysical and functional characterization of Norrin signaling through Frizzled4. *Proc. Natl. Acad. Sci. U. S. A.* 115, 8787−8792.

(45) Rovira, X., Vivo, M., Serra, J., Roche, D., Strange, P. G., and Giraldo, J. (2009) Modelling the interdependence between the stoichiometry of receptor oligomerization and ligand binding for a coexisting dimer/tetramer receptor system. *Br. J. Pharmacol.* 156, 28−35.

(46) Janda, C. Y., Waghray, D., Levin, A. M., Thomas, C., and Garcia, K. C. (2012) Structural basis of Wnt recognition by Frizzled. *Science* 337, 59−64.

(47) Povelones, M., and Nusse, R. (2005) The role of the cysteine-rich domain of Frizzled in Wingless- Armadillo signaling. *EMBO J.* 24, 3493−3503.

(48) Zhang, X., Dong, S., and Xu, F. (2018) Structural and Druggability Landscape of Frizzled G Protein- Coupled Receptors. *Trends Biochem. Sci.* 43, 1033−1046.

(49) DeBruine, Z. J., Xu, H. E., and Melcher, K. (2017) Assembly and architecture of the Wnt/beta-catenin signalosome at the membrane. *Br. J. Pharmacol.* 174, 4564−4574.

(50) Kozielewicz, P., Turku, A., and Schulte, G. (2020) Molecular Pharmacology of Class F Receptor Activation. *Mol. Pharmacol.* 97, 62−71.

(51) Miao, Y., Ha, A., de Lau, W., Yuki, K., Santos, A. J. M., You, C., Geurts, M. H., Puschhof, J., Pleguezuelos-Manzano, C., Peng, W. C., et al. (2020) Next-Generation Surrogate Wnts Support Organoid Growth and Deconvolute Frizzled Pleiotropy In Vivo. *Cell Stem Cell* 27, 840−851.

(52) Valnohova, J., Kowalski-Jahn, M., Sunahara, R. K., and Schulte, G. (2018) Functional dissection of the N- terminal extracellular domains of Frizzled 6 reveals their roles for receptor localization and Dishevelled recruitment. *J. Biol. Chem.* 293, 17875−17887.

(53) Weihs, F., Wang, J., Pfleger, K. D. G., and Dacres, H. (2020) Experimental determination of the bioluminescence resonance energy transfer (BRET) Forster distances of NanoBRET and red-shifted BRET pairs. *Anal Chim Acta X* 6, 100059.

(54) Eckert, A. F., Gao, P., Wesslowski, J., Wang, X., Rath, J., Nienhaus, K., Davidson, G., and Nienhaus, G. U. (2020) Measuring ligand-cell surface receptor affinities with axial line-scanning fluorescence correlation spectroscopy. *eLife* 9, 9.

(55) Lan, T. H., Liu, Q., Li, C., Wu, G., Steyaert, J., and Lambert, N. A. (2015) BRET evidence that beta2 adrenergic receptors do not oligomerize in cells. *Sci. Rep.* 5, 10166.

(56) Kozielewicz, P., Bowin, C. F., Turku, A., and Schulte, G. (2020) A NanoBRET-Based Binding Assay for Smoothened Allows Real-time Analysis of Ligand Binding and Distinction of Two Binding Sites for BODIPY-cyclopamine. *Mol. Pharmacol.* 97, 23−34.

(57) Proffitt, K. D., Madan, B., Ke, Z., Pendharkar, V., Ding, L., Lee, M. A., Hannoush, R. N., and Virshup, D. M. (2013) Pharmacological inhibition of the Wnt acyltransferase PORCN prevents growth of WNT-driven mammary cancer. *Cancer Res.* 73, 502−507.

(58) Willert, K. H. (2008) Isolation and application of bioactive Wnt proteins. *Methods Mol. Biol.* 468, 17−29.

(59) Cheng, Y., and Prusoff, W. H. (1973) Relationship between the inhibition constant (K1) and the concentration of inhibitor which causes 50% inhibition (I50) of an enzymatic reaction. *Biochem. Pharmacol.* 22, 3099−3108.